Supporting Online Material for

Hydrolytic catalysis and structural stabilization in a designed metalloprotein

Melissa L. Zastrow, Anna F. A. Peacock, Jeanne A. Stuckey, Vincent L. Pecoraro*

*To whom correspondence should be addressed. E-mail: vlpec@umich.edu

Materials and Methods, 1 Supplementary Discussion, 5 Supplementary Figures and 3 Supplementary Tables

Materials and Methods

Peptide synthesis and purification. Peptides were synthesized on an Applied Biosystems 433A peptide synthesizer, purified and characterized as previously reported.(*1*) Stock solutions of the apopeptides were prepared and their concentrations determined as previously reported.(*1*) Concentrations of **TRI**L23H for circular dichroism experiments were based on amino acid analysis performed by the Protein Structure Facility at the University of Michigan.

Circular Dichroism (CD) and UV-Visible (UV-Vis) spectroscopy. CD and UV-Vis spectra were recorded in quartz cuvettes at 25 °C on an AVIV 62DS spectrometer and Cary 100 Bio UV/Vis spectrometer, respectively. Guanidine hydrochloride CD titrations were performed at pH 8.5 as described previously.(*2*)

Crystallization, data collection, and refinement. Crystals of **CS**L9PenL23H were grown by vapour diffusion at 20 °C in a hanging drop with equal volumes of peptide (13.8 mg/ml **CS**L9PenL23H, 15 mM $Zn(OAc)_2$, 5 mM Tris pH 8.5) and precipitant (100 mM Imidazole pH 8.5, 28% PEG-8,000, 200 mM NaCl), and frozen in the mother liquor for data collection.

Data was collected at the Advanced Photon Source in the Argonne National Laboratory on the LS-CAT Beamline 21-ID-F equipped with a Mar 225 CCD (Mar USA, Evanston, IL) and at wavelength 0.97872 Å. One hundred and eighty frames of data were collected at -180 °C with a 1° rotation and 1-s exposure rate. Data were processed and scaled with the program HKL2000.(*3*) The crystals were of the space group $P2_1$ with unit cell parameters a = 25.88 Å b = 38.65 Å, c = 75.66 Å, $\alpha = \gamma = 90°$ and $\beta = 95.06°$.

The structures were solved by molecular replacement, with Phaser from the CCP4 suite(*4,5*), using as a model single α-helices based on pdb 3H5F.(*6*) The model was refined to 2.0 Å resolution with restrained refinement in Buster 2.8.0(*7*) and built in Coot(*8*). The final structure has a $R_{working}$ = 20.5% and R_{free} = 26.4%. The correlation coefficient plots calculated by Buster 2.8.0 indicate that the model structure is complete to 2.20 Å and the data does not show anisotropy. There are two independent trimers present in the asymmetric unit and fraying of the C-termini is observed, resulting in larger B-factors in this region. An overlay of the two trimers in the asymmetric unit demonstrates that they have similar overall folds and that the Zn(II) sites have the same geometry (Supplementary Fig. S3). To deduce the configuration of the metal sites, the atoms of these sites were initially refined without imposing geometric restraints. Once their positions were determined, geometric parameters were used to restrain the bond lengths and angles of the metal coordinating atoms (refer to Supplementary Table S2 for distances and angles of each metal site). Since the B-factors on several of the metals were

found to be higher than their coordinating atoms, the B-factors for these metals were set to the Wilson B for a round of occupancy refinement. The refined occupancies and accompanying B-values are shown in Supplementary Table S3. Omit maps of the metal sites confirmed a single position for each metal (i.e., no alternate positions for the metals were apparent in the density) (Supplementary Fig. S4). Data collection and refinement statistics are given in Table S3. The atomic coordinates and structure factors have been deposited in the Protein Data Bank with the ID code 3PBJ. Figures were generated in Pymol(*9*).

Determination of esterase activity. The esterase activities of $[Hg(II)]_S[Zn(II)(H_2O/OH^-)]_N(\mathbf{TRI}L9CL23H)_3^{n+}$ were determined spectrophotometrically with *p*-nitrophenyl acetate (*p*NPA, 0.03-1.2 mM) as substrate at 25 °C. Measurements were made at 348 nm, the isosbestic point for *p*-nitrophenol and *p*-nitrophenolate ion (ε = 5,000 $cm^{-1}M^{-1}$).(*10*) The observed activities were corrected for background ester hydrolysis in the absence of enzyme. A control containing $ZnSO_4$ without enzyme did not exhibit any activity above that of the blank. Activities were determined over the following range of pH's and conditions: pH 7.5-8.0, 50 mM HEPES, 0.1 M Na_2SO_4; pH 8.5-9.5, 50 mM CHES, 0.1 M Na_2SO_4. The substrate solution was prepared fresh each day beginning with a 0.1 M solution of *p*NPA in acetone and slowly adding doubly distilled H_2O (ddH_2O) with vigorous stirring to dilute to 3 mM *p*NPA. For measuring esterase activity: in a 1 mm pathlength spectrophotometric cuvette, buffer (50 mM), ddH_2O, and *p*NPA were mixed and the absorbance recorded (after baseline correction with solution containing only buffer and ddH_2O). Then, after addition of peptide (10 μM $ZnSO_4$ and 50 μM $[Hg(II)_S](\mathbf{TRI}L9CL23H)_3^-$, to ensure all Zn(II) was bound to the peptide), the increase in absorption at 348 nm was measured at least every 25 seconds for

at least 10 minutes, and longer for the slower rates at lower pH's. In addition to background correction for spontaneous hydrolysis in each buffer solution, the rates were corrected for background peptide activity (40 μM $[Hg(II)_S](\mathbf{TRI}L9CL23H)_3^-$, added to the control cuvette at the same time the catalyst, peptide-zinc complex, was added), as imidazole is known to modestly catalyze this reaction. Initial rates for each substrate concentration ([S], repeated at least twice per concentration per pH) were determined from linear fits of plots of product formation versus time. These slopes (or initial rates, ν) were then plotted as a function of [S] and their reciprocals taken to give double reciprocal or Lineweaver-Burke plots (fitted in OriginPro 8), from which V_{max}/K_M, V_{max}, and K_M values and their errors were determined based on the equation $1/\nu = 1/V_{max} + K_M/V_{max}[S]$. k_{cat} and k_{cat}/K_M values were determined based on the concentration of $[Hg(II)]_S[Zn(II)(H_2O/OH^-)]_N(\mathbf{TRI}L9CL23H)_3^{n+}$ catalyst, 10 μM. Similar values could be obtained by performing a non-linear fit of the initial rates to the Michaelis-Menten equation in Prism 5 (GraphPad Software). Note that k_{cat} and K_M values have rather large errors due to the solubility limitations of *p*NPA, which precluded our ability to test substrate concentrations at or above the K_M values (the highest achievable under our conditions was 1.2 mM). pK_a's were determined from fits of k_{cat}/K_M and k_{cat} vs. pH in OriginPro 8 and the reported errors are based on these fits. The same procedure was used for measuring the activity of $[Zn(II)]_N(\mathbf{TRI}L23H)_3^{2+}$. For inhibition studies, the above procedure was also followed, with the exception that varying concentrations of potassium acetate (0, 0.2, 0.5, 0.7 M) were included in the initial buffer solution before addition of substrate and then enzyme. The catalytic efficiencies of several controls were also determined (and are summarized in Supplementary Table S4 and discussed in the Supplementary Discussion). For $[Hg(II)_S](\mathbf{TRI}L9CL23H)_3^-$ and apo$(\mathbf{TRI}L9CL23H)_3$ (pH 9.0), 40 μM of peptide complex was used and run in parallel with spontaneous *p*NPA

hydrolysis as the control and the rates corrected for this. The approach taken for $[Hg(II)]_S[Zn(II)(OH^-)]_N$(**CS**L9PenL23H)$_3$ (pH 9.5) was identical to that used for $[Hg(II)]_S[Zn(II)(OH^-)]_N$(**TRI**L9CL23H)$_3$. Finally, the activity of $[Hg(II)]_S$(**TRI**L9C)$_3^-$ + Zn(II) (50 μM total, 10 μM $ZnSO_4$) was measured as an unbound Zn(II) control at pH 9.0 and compared to that of $[Hg(II)]_S$(**TRI**L9C)$_3^-$ (40 μM), both of which were corrected for spontaneous hydrolysis. Catalytic efficiencies (k_{cat}/K_M) of all of the above controls could be successfully determined both utilizing Lineweaver-Burke plots as described above and non-linear fits of the initial rates to the Michaelis-Menten equation in Prism 5 (GraphPad Software). However, as considerable errors were observed for individual k_{cat} and K_M values, these are not reported.

Determination of carbon dioxide hydration activity. Initial rates of CO_2 hydration catalyzed by $[Hg(II)]_S[Zn(II)(OH^-)]_N$(**TRI**L9CL23H)$_3$ were measured at 25.0 °C in an OLIS RSM Stopped Flow Spectrophotometer using the changing pH-indicator method.[11] The buffer/indicator pair used was CHES/thymol blue (pH 9.5, 590 nm). The ionic strength of the buffer was maintained at 0.1 M with Na_2SO_4. Saturated solutions of CO_2 (Matheson Tri-Gas, Inc., Research Grade) were prepared by bubbling the gas through deionized, distilled water. Dilutions were made using gas-tight syringes and a final check of the CO_2 concentration was possible during the experiment.[11] The buffer factor was determined following Khalifah's method and closely matched that which could be calculated theoretically, 0.08. CO_2 concentrations ranged from 2.0-19.0 mM. Buffer concentration was maintained at 50 mM in the reaction cell. All rates measured on the stopped-flow spectrophotometer were initiated by rapid 1:1 mixing of the substrate with a buffer/indicator solution containing the desired catalyst (water for the spontaneous reaction and 10 μM $ZnSO_4$ + 50 μM $[Hg(II)_S]$(**TRI**L9CL23H)$_3^-$ for the catalyzed reaction, as for the esterase assays) and monitored over a very short time interval in order to record

only the initial linear portion of the reaction. At least four replicates were performed for each substrate concentration. Initial rates, ν, were plotted as a function of [S] and their reciprocals taken to give double reciprocal or Lineweaver-Burke plots (fitted in OriginPro 8), from which V_{max}/K_M, V_{max}, and K_M values and their errors were determined based on the equation $1/v = 1/V_{max} + K_M/V_{max}[S]$. k_{cat} and k_{cat}/K_M values were determined based on the concentration of $[Hg(II)]_S[Zn(II)(OH^-)]_N$(**TRI**L9CL23H)$_3$ catalyst, 10 μM. All reported rates account for the uncatalyzed background reaction. Rates due to excess (not Zn(II)-bound) peptide, $[Hg(II)_S]$(**TRI**L9CL23H)$_3^-$ were negligible compared to the background. The kinetic parameters were verified using a non-linear fit to the Michaelis-Menten equation in Prism 5 (GraphPad Software).

Supplementary Discussion

As discussed in the main text, $[Hg(II)]_S[Zn(II)(OH^-)]_N$(**TRI**L9CL23H)$_3$ exhibits a catalytic efficiency of 23.3 ± 0.03 M^{-1} s^{-1} at pH 9.5 and of 17.6 ± 0.03 M^{-1} s^{-1} at pH 9.0. Importantly, in the presence of Hg(II), but in the absence of Zn(II), an efficiency of only 6.0 ± 0.1 M^{-1} s^{-1} was measured at pH 9.0 (Supplementary Table S4). In the absence of both metals, apo(**TRI**L9CL23H)$_3$ exhibits an identical catalytic efficiency. These both represent about 34% of the activity of the Zn(II)-bound version. The fact that the values are the same in the presence and absence of Hg(II) indicates that this activity is due primarily to the three His residues in the trimer acting as catalysts. This observation is within a factor of two of the catalytic efficiency for His-based hydrolysis of *p*NPA reported by Bolon and Mayo.[12] The rate of apo-CA towards *p*NPA hydrolysis has not been typically reported in the literature as a catalytic efficiency or second order rate constant value. Typically, the background activity is measured using the acetazolamide-inhibited enzyme, in which case the free imidazole residues are still bound to Zn(II) and therefore not available to contribute to catalysis. It should be noted however, that while this somewhat considerable amount of apopeptide activity is observed for *p*NPA hydrolysis, negligible apopeptide activity is actually observed for the physiologically relevant reaction, CO_2 hydration.

In order to determine the activity of an unbound Zn(II) control peptide (that is, with Zn(II) present but not bound in the designed His_3 site), **TRI**L9C was used. This peptide has Leu residues in place of His at the 23rd position. $[Hg(II)]_S$(**TRI**L9C)$_3^-$ and $[Hg(II)]_S$(**TRI**L9C)$_3^-$ + Zn(II) were run in parallel. The difference between the two rates is essentially negligible (k_{cat}/K_M values were 1.9 ± 0.3 M^{-1} s^{-1} in the absence of Zn(II) and 1.8 ± 0.2 M^{-1} s^{-1} in its presence (Supplementary Table S4)). These results support the

conclusion that Zn(II) must be bound to the designed His_3 site to observe the reported high activity.

A denatured control experiment was performed at pH 9.0 in the presence of ~4.8 M GuaHCl. For this experiment, the initial rate at only a single concentration of *p*NPA (500 μM) was determined and corrected for spontaneous background hydrolysis. Approximately 12% activity in the presence of Zn(II) is observed over the $[Hg(II)_S](\mathbf{TRI}L9CL23H)_3^-$ peptide without Zn(II). From the guanidinium denaturation curve, the peptide is approximately 6% folded at this concentration (using an ideal ellipticity of -35,500 to calculate percent folding). Given that the activity and the folding percentages are within experimental error, it is expected that the residual activity observed is due to the residual folded peptide.

Notably, the activity of the crystallographic analog $[Hg(II)]_S[Zn(II)(OH^-)]_N(\mathbf{CS}L9PenL23H)_3$ was measured at pH 9.5 and, after correcting for the folding concentration, a catalytic efficiency of 20.2 ± 2.3 M^{-1} s^{-1} is obtained. This compares well to that for $[Hg(II)]_S[Zn(II)(OH^-)]_N(\mathbf{TRI}L9CL23H)_3$, which is 23.3 ± 0.3 M^{-1} s^{-1}.

There are some designed nucleophilic catalysts which, while not meant to be CA models, do represent important designed protein catalysts for *p*NPA hydrolysis. Broo *et al.*[13,14] reported a designed helix-loop-helix dimer, KO-42, which contains six His residues that contribute to a second-order rate constant of 0.29 M^{-1} s^{-1} at pH 5.1. This value can be extrapolated to ~0.7 M^{-1} s^{-1} at pH 7, based on the pH rate profiles reported for similarly activated esters.[12] Bolon and Mayo[12] have reported the redesign of thioredoxin to include an active site to support His-mediated nucleophilic hydrolysis of *p*NPA. At pH 7, PZD2 has a catalytic efficiency of 2.7 M^{-1} s^{-1}. By comparison, $[Hg(II)]_S[Zn(II)(H_2O/OH^-)]_N(\mathbf{TRI}L9CL23H)_3^+$ exhibits a relatively similar catalytic

efficiency at pH 7.5 (1.38 M^{-1} s^{-1}). It is expected that in these His-catalyzed systems, the His residues are completely deprotonated by pH 7. In our system, however, there is not a high proportion of the active species at low pH. The activity increases with increasing pH as the Zn(II)-bound water is deprotonated to form the Zn(II)-OH^- nucleophile. Therefore, if we compare the activity of $[Hg(II)]_S[Zn(II)(OH^-)]_N$(**TRI**L9CL23H)$_3$ at its maximal value (pH 9.5, 23.3 M^{-1} s^{-1}) to those of the designed proteins discussed above, we find that our system performs this reaction with a ~10-fold enhanced catalytic efficiency.

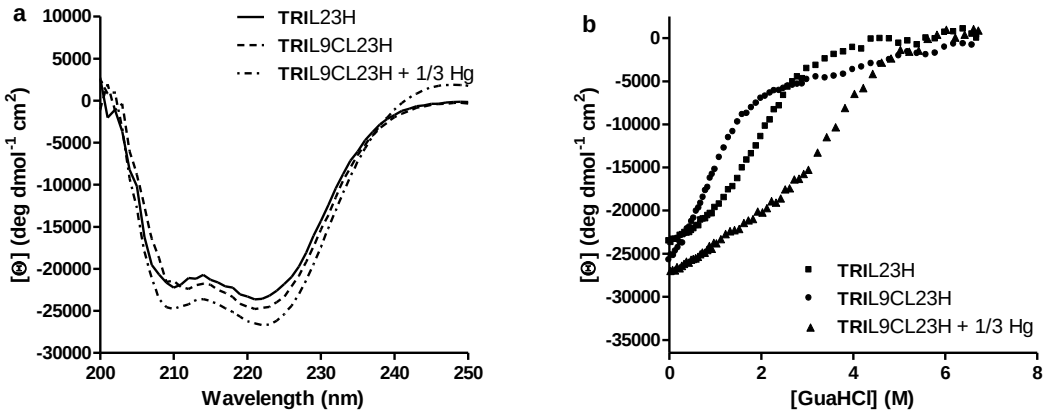

Figure S1 | Folding of TRIL23H, TRIL9CL23H, and TRIL9CL23H + 1/3 Hg(II) as monitored by CD. a, CD spectra of **TRI**L23H (—), **TRI**L9CL23H (⁻ ⁻), and **TRI**L9CL23H + 1/3 Hg(II) (⁻ **-** ⁻) at pH 8.5 and ambient temperature. **b,** Guanidine hydrochloride denaturation titrations represented by the molar ellipticity values [Θ] at 222 nm versus denaturant concentration for **TRI**L23H (■), **TRI**L9CL23H (●), and **TRI**L9CL23H + 1/3 Hg(II) (▲), respectively. Addition of Hg(II) to **TRI**L23H does not result in additional stabilization (not shown). We have refrained from giving a quantitative determination of free energy values because the denaturation curve for **TRI**L9CL23H does not level off at zero concentration of denaturant. For the **TRI**L9CL23H + 1/3 Hg(II) curve, competition of chloride with the sulfur ligands may lead to a decrease in stability so that what is observed is a minimum value for Hg(II) folding and therefore, the system is too complicated to fit to a simple two-state folding unfolding model. Nonetheless, the midpoint has shifted dramatically, demonstrating the stability enforced by Hg(II) binding.

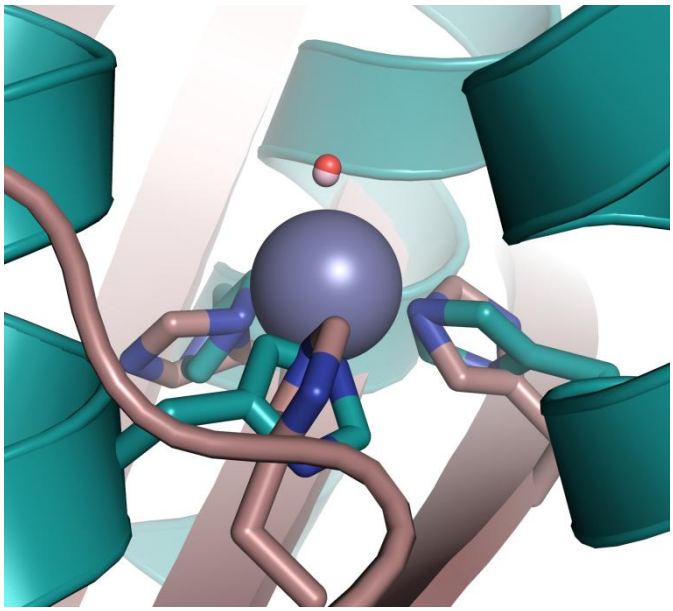

Figure S2 | Overlay of the Zn(II)N_3O site in [Hg(II)]$_S$[Zn(II)(H_2O/OH^-)]$_N$(CSL9PenL23H)$_3^{n+}$ with the active site of human CAII. [Hg(II)]$_S$[Zn(II)(H_2O/OH^-)]$_N$(**CS**L9PenL23H)$_3^{n+}$ (pdb 3PBJ) is shown in cyan and CAII in tan (pdb 2CBA). The solvent molecule associated with [Hg(II)]$_S$[Zn(II)(H_2O/OH^-)]$_N$(**CS**L9PenL23H)$_3^{n+}$ is shown in red and that associated with CAII in pale pink. As discussed in the main text, Figure 2, the model displays an excellent structural overlay for the first coordination sphere atoms with CAII. Overlay was performed manually in Pymol.

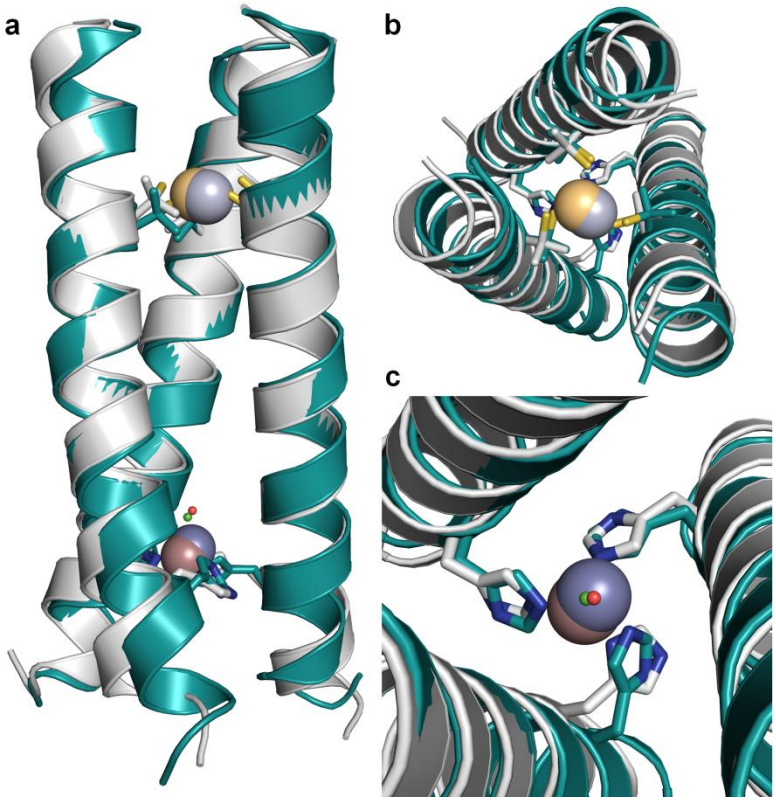

Figure S3 | Overlay of the two different 3-helix bundles in the asymmetric unit of $[Hg(II)]_S[Zn(II)(H_2O/OH^-)]_N(CSL9PenL23H)_3^{n+}$. The 3SCC containing chains ABC (with the trigonal $Hg(II)S_3$ site and $Zn(II)N_3Cl$ sites) is colored grey (main chain atoms), tan (zinc atom), green (chloride), and yellow (mercury atom). The 3SCC containing chains DEF (T-shaped $Hg(II)S_3$ and $Zn(II)N_3O$) is colored cyan (main chain atoms). **a,** Overlay of the two trimers, as performed manually in Pymol. **b,** a top-down view of the 3-helix bundles, focusing on the $Hg(II)S_3$ sites. **c,** a close-up top-down view of the two $Zn(II)N_3X$ sites. The overlay of the two trimers demonstrates that, even though there are slight differences in the mercury sites (T-shaped or trigonal) and zinc sites ($Zn(II)N_3O$ or $Zn(II)N_3Cl$), the overall fold remains essentially identical. It is also apparent that the C-terminal ends of the trimers (where the Zn(II) sites are) display a higher degree of "fraying", as compared to the N-terminal ends.

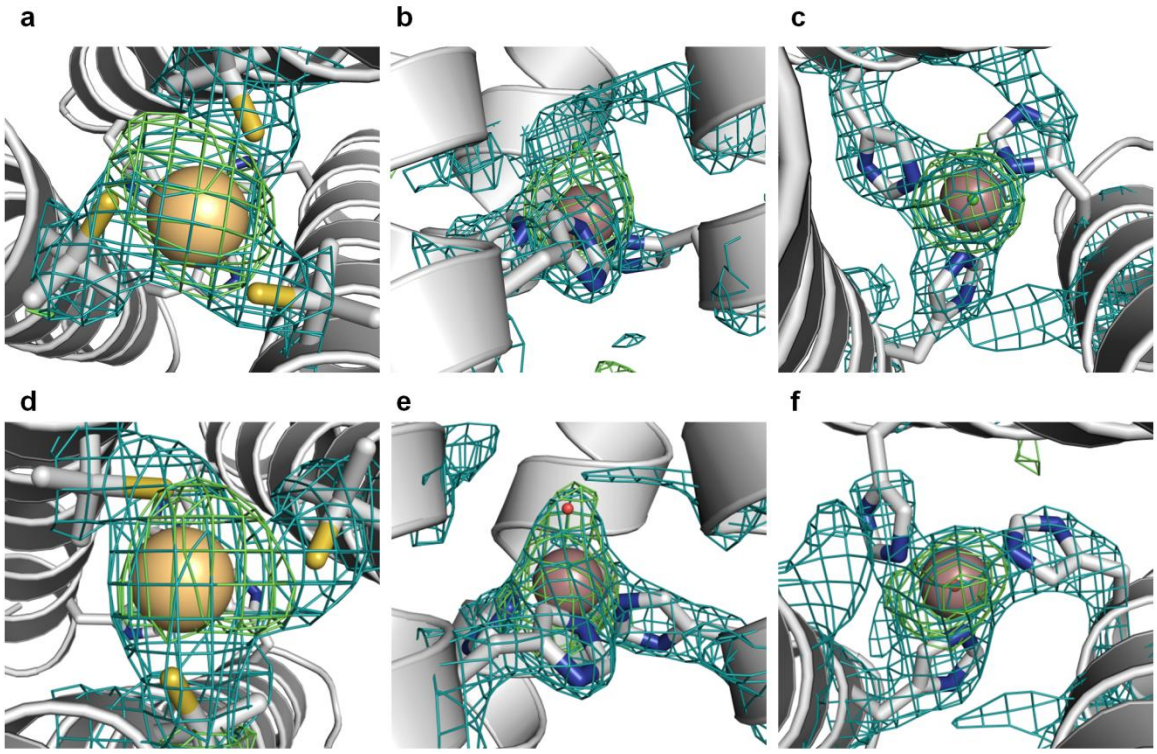

Figure S4 | Omit maps for the metal sites in $[Hg(II)]_S[Zn(II)(H_2O/OH^-)]_N(CSL9PenL23H)_3^{n+}$. Shown are the main chain atoms represented as helical ribbons (light grey) and the Pen and His side chains in stick form (sulfur = yellow, nitrogen = blue, oxygen = red, chloride = green). The mercury atom is colored light orange and zinc is colored tan. Electron density maps were generated through refinement with the metal occupancies set to zero. $2F_o$-F_c electron density is shown for each metal site contoured at 1.5 σ and colored blue. F_o-F_c electron density is shown for each metal contoured at 3 σ and colored green. **a,** Top-down view of the trigonal $Hg(II)S_3$ site, **b,** side view of the $Zn(II)N_3Cl$ site, **c,** top-down view of the $Zn(II)N_3Cl$ site, **d,** top-down view of the T-shaped $Hg(II)S_3$ site, **e,** side view of the $Zn(II)N_3O$ site, **f,** top-down view of the $Zn(II)N_3O$ site. No evidence of alternate ligand-metal geometries or metal positions is observed.

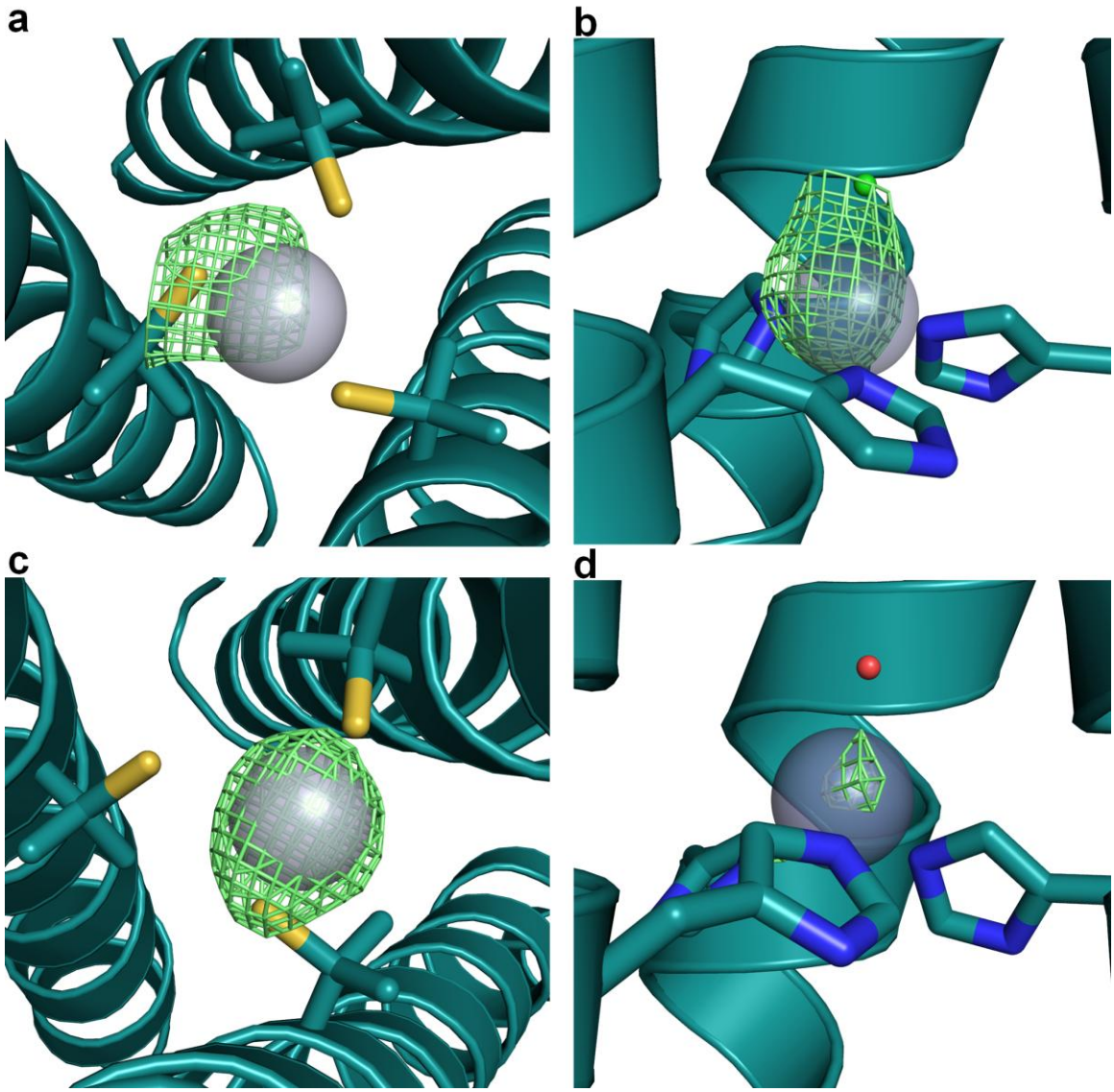

Figure S5 | Metal difference density as observed at the start of refinement. Shown are the metal difference electron densities (F_o-F_c) contoured at 3.0 σ for each site in each trimer in the asymmetric unit. **a,** Trigonal Hg(II)S_3 site, **b,** Zn(II)N_3Cl site, **c,** T-shaped Hg(II) site, **d,** Zn(II)N_3O site. These confirm that the metal positions at the end of refinement are the same as they were at the start.

Table S1 | Peptide sequences used in these studies.

Peptide		a b c d e f g	a b c d e f g	a b c d e f g	a b c d e f g	
TRIL23H	Ac-G	LKALEEK	LKALEEK	LKALEEK	**H**KALEEK	G-NH_2
TRIL9C	Ac-G	LKALEEK	**C**KALEEK	LKALEEK	LKALEEK	G-NH_2
TRIL9CL23H	Ac-G	LKALEEK	**C**KALEEK	LKALEEK	**H**KALEEK	G-NH_2
CSL9PenL23H	Ac-E	WEALEKK	**Pen**AALESK	LQALEKK	**H**EALEHG	-NH_2

C- and N-termini are capped by Ac and NH_2 groups, respectively.

Table S2 | Metal-ligand bond distances and angles in $[Hg(II)]_S[Zn(II)(H_2O/OH^-)]_N(CSL9PenL23H)_3^{n+}$.

$Zn(II)N_3Cl$ site		**$Hg(II)S_3$ trigonal**		**$Zn(II)N_3O$ site**		**$Hg(II)S_3$ t-shaped**	
bond distances (Å)[1]							
$Zn\text{-}N_A$	1.94	$Hg\text{-}S_A$	2.21	$Zn\text{-}N_D$	1.96	$Hg\text{-}S_D$	2.29
$Zn\text{-}N_B$	1.92	$Hg\text{-}S_B$	2.07	$Zn\text{-}N_E$	2.02	$Hg\text{-}S_E$	2.13
$Zn\text{-}N_C$	1.92	$Hg\text{-}S_C$	2.41	$Zn\text{-}N_F$	2.03	$Hg\text{-}S_F$	3.06
Zn-Cl	2.24			Zn-O	2.18		
bond angles (°)							
$N_A\text{-}Zn\text{-}N_B$	115.66	$S_A\text{-}Hg\text{-}S_B$	135.80	$N_D\text{-}Zn\text{-}N_E$	101.77	$S_D\text{-}Hg\text{-}S_E$	160.11
$N_B\text{-}Zn\text{-}N_C$	125.14	$S_B\text{-}Hg\text{-}S_C$	115.65	$N_E\text{-}Zn\text{-}N_F$	114.48	$S_E\text{-}Hg\text{-}S_F$	90.55
$N_A\text{-}Zn\text{-}N_C$	95.52	$S_A\text{-}Hg\text{-}S_C$	108.26	$N_D\text{-}Zn\text{-}N_F$	93.32	$S_D\text{-}Hg\text{-}S_F$	106.52
$N_A\text{-}Zn\text{-}Cl$	96.00			$N_D\text{-}Zn\text{-}O$	129.01		
$N_B\text{-}Zn\text{-}Cl$	119.51			$N_E\text{-}Zn\text{-}O$	111.34		
$N_C\text{-}Zn\text{-}Cl$	98.98			$N_F\text{-}Zn\text{-}O$	106.07		

[1]Subscripts represent which helix chain the ligand belongs to (the ligands are 'N' for the nitrogen of Histidine and 'S' for the sulfur of Penicillamine).

Table S3 | Data collection and refinement statistics.

Data collection	
Space group	$P2_1$
Cell dimensions	
***a*, *b*, *c* (Å)**	25.88, 38.65, 75.66
***α*, *β*, *γ* (°)**	90, 95.06, 90
Wavelength (Å)	0.97872
Resolution (Å)[1]	2.2(2.24-2.20)
R_{sym} **(%)**[2]	5.8(32.1)
<I/σI>[3]	>20(2)
Completeness (%)[4]	98.3(97.1)
Redundancy	3.0(2.9)
Beamline	LS-CAT 21-ID-F
Refinement	
Resolution (Å)	2.20(26.98-2.20)
No. reflections	7625
R_{factor} **(%)**[5]	20.5
R_{free} **(%)**[6]	26.4
No. atoms	
Protein[7]	1359
Ligand/ion	13
Water	66
RSCC/RSR for metal sites[8]	
Zn(II) in ZnN_3Cl site	0.969/0.046
Cl^- in ZnN_3Cl site	0.952/0.122
Zn(II) in ZnN_3O site	0.926/0.104
Hg(II) in trigonal site	0.851/0.085
Hg(II) in T-shaped site	0.955/0.087
Occupancies of metal sites/B-factors[9]	
Zn(II) in ZnN_3Cl site	1.0/41.77
Zn(II) in ZnN_3O site	1.0/76.96
Hg(II) in trigonal site	0.55/54.73
Hg(II) in T-shaped site	0.60/46.36
B-factors[9]	
Protein	51.4
Ligand/ion	55.1
Water	51.1
R.m.s deviations[10]	
Bond lengths (Å)	0.014
Bond angles (°)	1.73

[1]Statistics for highest resolution bin of reflections in parentheses.

[2]$R_{sym} = \Sigma_h\Sigma_j \mid I_{hj} - \langle I_h \rangle \mid / \Sigma_h\Sigma_j I_{hj}$, where I_{hj} is the intensity of observation j of reflection h and $\langle I_h \rangle$ is the mean intensity for multiply recorded reflections.

[3]Intensity signal-to-noise ratio.
[4]Completeness of the unique diffraction data.
[5]$R_{factor} = \Sigma_h$ I IFoI – IFcI I / Σ_hIFoI, where Fo and Fc are the observed and calculated structure factor amplitudes for reflection h.
[6]R_{free} is calculated against a 10% random sampling of the reflections that were removed before structure refinement.
[7]Total number of protein atoms refined in the asymmetric unit.
[8]Real-space correlation coefficient (RSCC) and real-space R values (RSR) as obtained from the Uppsala Electron Density Server.(*15*)
[9]B factors are higher than what is typically expected for a refined crystal structure. We believe this is due to the fraying of the C-termini. Due to the fraying, three very similar molecular replacement solutions for this structure were seen, the clearest of which was used for refinement of the structure presented here. Notably, the core residues including the metal positions were virtually identical in all solutions.
[10]Root mean square deviation of bond lengths and bond angles.

Table S4 | Comparisons of the kinetics for *p*-nitrophenyl acetate hydrolysis by selected catalysts at 25 °C.

Catalyst	pK_a[1]	pH	k_{cat}/K_M ($M^{-1} s^{-1}$)	k_2 ($M^{-1} s^{-1}$)
$[Hg(II)]_S[Zn(II)(OH^-)]_N$	8.8	9.5	23.3 ± 0.3	
(**TRI**L9CL23H)$_3$		9.0	17.6 ± 0.3	
$[Hg(II)]_S[Zn(II)(H_2O)]_N$ (**TRI**L9CL23H)$_3^+$	8.8	7.5	1.38 ± 0.04	
$[Hg(II)_S]$(**TRI**L9CL23H)$_3^-$	-	9.0	6.0 ± 0.1	
apo(**TRI**L9CL23H)$_3^{3-}$	-	9.0	6.0 ± 0.1	
$[Zn(II)]_N$(**TRI**L23H)$_3^{2+}$	9.0	9.0	14.1 ± 0.3	
$[Hg(II)]_S[Zn(II)(OH^-)]_N$ (**CS**L9PenL23H)$_3^{n+}$	ND	9.5	20.2 ± 2.3[2]	
$[Hg(II)]_S$(**TRI**L9C)$_3^-$	-	9.0	1.9 ± 0.3	
$[Hg(II)]_S$(**TRI**L9C)$_3^-$+Zn(II)	-	9.0	1.8 ± 0.2	
CAII[3]	6.8	9.0	2320	
CAI[3]	7.3	9.0	370	
[12]aneN_3[4]	7.3	8.2		0.041
[15]aneN_3O_2[5]	8.8			0.6
tris(4,5-di-*n*-propyl-2-imidazolyl) phosphine	8.7			0.86/0.0186[6]
[12]aneN_4[7]	7.9	9.3		0.1
[12]aneN_4 hexadecyl derivative[8]	7.56	10.5		5
KO-42	-	5.1/7.0		0.29/~0.7[9]
PZD2[10]	-	7.0	2.7	

[1]For deprotonation of Zn(II)-OH_2 to form catalytically active Zn(II)-OH in Zn(II)N_X (in CA and CA-like models).

[2]Normalized according to the folding concentration of $[Hg(II)_S]$(**CS**L9PenCL23H)$_3^-$ relative to $[Hg(II)_S]$(**TRI**L9CL23H)$_3^-$.

[3]Taken from ref. S10.

[4]Taken from ref. S16.

[5]Estimated by extrapolating to the 100% active Zn(II)-OH^- form of the complex from pH-dependent data (ref. S17).

[6]The former value is that measured in micellar medium; the latter estimated under aqueous conditions (ref. S18).

[7]Taken from ref. S19.

[8]Taken from ref. S20.

[9]*De novo* designed four-helix bundle containing six His residues that contribute to a second-order rate constant and whose value at pH 7.0 is extrapolated from the reported value at pH 5.1 of 0.29 $M^{-1}s^{-1}$ using pH rate profiles reported for similarly activated esters (ref. S12-S14).

[10]A computationally redesigned thioredoxin to include a nucleophilic His residue (ref. S12).

References

S1. B. T. Farrer, N. P. Harris, K. E. Balchus & V. L. Pecoraro. Thermodynamic model for the stabilization of trigonal thiolato mercury(II) in designed three-stranded coiled coils. *Biochemistry* **40,** 14696-14705 (2001).

S2. G. R. Dieckmann *et al.* The role of protonation and metal chelation preferences in defining the properties of mercury-binding coiled coils. *J. Mol. Biol.* **280,** 897-912 (1998).

S3. Z. Otwinowski & W. Minor. Processing of X-ray diffraction data collected in oscillation mode. *Methods Enzymol.* **276,** 307-326 (1997).

S4. E. Potterton, P. Briggs, M. Turkenburg & E. Dodson. A graphical user interface to the *CCP*4 program suite. *Acta Cryst. D* **59,** 1131-1137 (2003).

S5. A. J. McCoy *et al. Phaser* crystallographic software. *J. Appl. Cryst.* **40**, 658-674 (2007).

S6. A. F. A. Peacock, J. A. Stuckey & V. L. Pecoraro. Switching the chirality of the metal environment alters the coordination mode in designed peptides. *Angew. Chem. Int. Ed.* **48,** 7371-7374 (2009).

S7. G. Bricogne *et al.* (2010). BUSTER version 2.8.0. Cambridge, United Kingdom: Global Phasing Ltd.

S8. Emsley, P. & Cowtan, K. *Coot*: model-building tools for molecular graphics. *Acta Cryst. D* **20,** 2126-2132 (2004).

S9. W. L. DeLano, The PyMol Molecular Graphics System, DeLano Scientific, Palo Alto, California, USA (2005). http://www.pymol.org

S10. J. A. Verpoorte, S. Mehta & J. T. Edsall. Esterase activities of human carbonic anhydrases B and C. *J. Biol. Chem.* **242,** 4221-4229 (1967).

S11. Khalifah, R. G. The carbon dioxide hydration activity of carbonic anhydrase. *J. Biol. Chem.* **246**, 2561-2573 (1971).

S12. Bolon, D. N. & Mayo, S. L. Enzyme-like proteins by computational design. *Proc. Natl. Acad. Sci. U.S.A.* **98**, 14274-14279 (2001).

S13. Broo, K., Brive, L., Ahlberg, P., & Baltzer, L. Catalysis of hydrolysis and transesterification reactions of *p*-nitrophenyl esters by a designed helix-loop-helix dimer. *J. Am. Chem. Soc.* **119**, 11362-11372 (1997).

S14. Nilsson, J. & Baltzer, L. Reactive-site design in folded-polypeptide catalysts-the leaving group pK_a of reactive esters sets the stage for cooperativity in nucleophilic and general-acid catalysis. *Chem. Eur. J.* **6**, 2214-2220 (2000).

S15. G. J. Kleywegt *et al. Acta Cryst.* The Uppsala electron-density server. *D* **60,** 2240-2249 (2004).

S16. Kimura, E., Shiota, T., Koike, T., Shiro, M. & Kodama, M. A Zinc(II) Complex of 1,5,9-triazacyclododecane ([12]aneN_3) as a model for carbonic anhydrase. *J. Am. Chem. Soc.* **112,** 5805-5811 (1990).

S17. Bazzicalupi, C. *et al.* Carboxy and phosphate esters cleavage with mono- and dinuclear zinc(II) macrocyclic complexes in aqueous solution. Crystal structure of $[Zn_2L1(\mu\text{-}PP)_2(MeOH)_2](ClO_4)_2$ (L1 = [30]aneN_6O_4, PP^- = diphenyl phosphate). *Inorg. Chem.* **36,** 2784-2790 (1997).

S18. Koerner, T. B. & Brown, R. S. The hydrolysis of an activated ester by a tris(4,5-di-*n*-propyl-2-imidazolyl)phosphine-Zn^{2+} complex in neutral micellar medium as a model for carbonic anhydrase. *Can. J. Chem.* **80,** 183-191 (2002).

S19. Koike, T., Takamura, M., & Kimura, E. Role of zinc(II) in *β*-lactamase II: a model study with a zinc(II)-macrocyclic tetraamine (1,4,7,10-tetraazacyclododecane, cyclen) complex. *J. Am. Chem. Soc.* **116,** 8443-8449 (1994).

S20. Kimura, E., Hashimoto, H., & Koike, T. Hydrolysis of lipophilic esters catalyzed by a zinc(II) complex of a long alkyl-pendant macrocyclic tetraamine in micellar solution. *J. Am. Chem. Soc.* **118,** 10963-10970 (1996).